Journal of Engineering Science and Technology
Vol. 12, No. 4 (2017) 1037 - 1047

ANALYSIS OF INTERGRANULAR CARBIDE PRECIPITATE IN HAZ OF MARTENSITIC STAINLESS STEEL

ISMAILA I. AHMED[1,*], JELEEL A. ADEBISI[2], SULAIMAN ABDULKAREEM[3], ANDREW H. SHERRY[1]

[1]Material Performance Centre, University of Manchester, Oxford Road, Manchester, M13 9PL, UK
[2]Department of Materials and Metallurgical Engineering, University of Ilorin, P.M.B. 1515, Nigeria
[3]Department of Mechanical Engineering, University of Ilorin, P.M.B. 1515, Nigeria
*Corresponding Author: ismaila.ahmed@yahoo.com

Abstract

Analysis of intragranular carbide precipitate in the Heat Affected Zone (HAZ) of Martensitic Stainless Steel (MSS) weldment was carried out. Low carbon grade martensitic stainless steel weldment subjected to four point bend test in simulated sweet crude environment was analysed with Transmission Electron Microscope (TEM). The optical microscopy of the failed sample revealed the presence of intergranular cracks on both sides of the weldment in the HAZ. Electron transparent sample for TEM was prepared from the HAZ of the weldment using extraction replica technique. The examination of TEM specimen in imaging mode revealed the presence of precipitates on grain boundaries. The compositional analysis of the precipitates was carried out with Energy Dispersive X-ray (EDX). The result of EDX analysis showed the presence of chromium and molybdenum, this suggests, the precipitates were carbides of the form $M_{23}C_6$. The study therefore upholds sensitisation as the mechanism behind the intergranular cracks observed in the HAZ of the MSS weldment.

Keywords: Carbide, Crack, Extraction Replica, Stainless steel, Sensitisation, Weld.

1. Introduction

High carbon grades of Martensitic Stainless Steels (MSSs) have been used in the past as down hole tubular for oil and gas transportations in sweet (H_2S free) environments at elevated temperatures of about 110°C, but the high carbon content poses threats to its weldability. Its heat affected zones have suffered from

Nomenclatures

4PBT	Four Point Bend Test
EN	Electrode Negative
EP	Electrode Positive
W2AVII	Sample Name

Greek Symbols

ϕ	Diameter of the filler wire (Table 1)

Abbreviations

DC	Direct Current
DCRP	Direct Current Reverse Polarity
EDX	Energy Dispersive X-ray
GMAW	Gas Metal Arc Welding
HAZ	Heat Affected Zone
LHS	Left Hand Side
MSS	Martensitic Stainless Steel
PGMA	Pulsed Gas Metal Arc
PWHT	Post Weld Heat Treatment
RHS	Right Hand Side
SCC	Stress Corrosion Cracking
TEM	Transmission Electron Microscope
TWI	The Welding Institute

cracks due to high hardness. The use of MSS in sour environments containing H_2S also suffers from cracks believed to be caused by hydrogen embrittlement [1]. In recognition of these problems, steels manufacturers have come up with modified low carbon 13%Cr MSS. The steels have the same Cr contents but with less than 0.02%C and other alloys such as Ni and Mo have been added in a significant amount to enhance corrosion resistance of the steels. The low C content enables the steels to be welded without preheating and Post Weld Heat Treatment (PWHT) [2]. Hence, they became one of the most widely used piping steel materials for oil and gas transportation [3, 4].

However, despite the benefits of the MSS in pipeline transportation, they are still susceptible to thermal aging embrittlement [5] and localised corrosion including Stress Corrosion Cracking (SCC) [4, 6]. Stress Corrosion Cracking is caused by the action of mechanical (including residual) stresses on susceptible materials in an aggressive environment. Welded joints are quite vulnerable to SCC due to sensitization (intergranular precipitation of Cr, Fe-Carbides along the prior austenite grain boundary) of the weld microstructures and the presence of internal stresses [7-9]. The objective of the study was to carry out compositional analysis of intragranular carbide precipitate in the Heat Affected Zone (HAZ) of MSS weldment. This was achieved through girth welding of martensitic stainless steel pipe and the use of extraction replica technique to obtained intergranular carbide precipitates from HAZ for analysis with TEM and EDX.

2. Experimental Procedure

2.1. Materials

The materials used for the research study was low carbon martensitic stainless steels. The materials were provided as-welded by The Welding Institute, (TWI) Cambridge, United Kingdom. The original martensitic stainless steel pipe without any welding heat input is referred to as the parent steel and the filler wire used for fabrication was superduplex stainless steel. The superduplex filler wire is selected for enhanced corrosion resistance of the weld metal and matching strength with MSS, but care must be taken if postweld heat treatment must be done to avoid loss of toughness close to fusion boundary line [10-12]. The detailed chemical compositions of the parent and filler metals are shown in Table 1.

Table 1. Chemical composition of the specimens used (parent material and the filler wire).

	Element, wt %									
Description	**C**	**N**	**Si**	**Mn**	**P**	**Ti**	**Cr**	**Mo**	**Ni**	**Al**
Parent steels	0.009	0.005	0.20	0.43	0.014	0.120	12.20	2.51	6.40	0.03
Filler(1.2 mm ϕ)	0.027	0.232	0.40	0.41	0.016	NA	26.10	3.90	9.30	NA

2.2. Girth welding of MSS pipes

Mechanised Pulsed Gas Metal Arc (PGMA) welding process was used for the fabrication of the MSS pipes at TWI, Cambridge. The PGMA welding process is notable for significantly lower welding porosity. The Gas-metal arc welding process used 1.2 mm diameter superduplex stainless steel (detailed composition in Table 1) as continuous filler wire electrode and an externally supplied inert shielding gases comprising Ar/He/CO_2/N_2. The consumable wire electrode produced an arc with the work piece which formed part of the electric circuit and provided filler to the weld joint. Wire was fed to the arc by an automatic wire feeder.

The externally supplied shielding gas played dual roles in GMAW. Firstly, it protects the arc, the molten metal, and cooling weld metal from impurities in the air and secondly, it provides desired arc characteristics through its effect on ionisation. The DC-EP (or DC-RP) was used because it ensures electrons are accelerated from negative work piece onto the positive electrode with sufficient energy to melt the filler wire [7]. The schematic diagram of the weldment is shown in Fig. 1. Three different microstructural zones exist in the weldment characterised by the welding heat namely: the parent material, the HAZ and the weld metal affected by dilution during high temperature fusion.

2.3. Four point bend test

Transverse section of as-welded specimen (W2AVII) of dimensions 100×15×3 mm^3 was sectioned from the welded girth ring with root surface left intact. The samples had been subjected to Four Point Bend (4PB) Test during which the specimens was stressed to about 100% of the measured 0.2% yield strength in bolt-loaded jigs, to provide the necessary strain in the weldment toe and HAZ

areas. Strain gauges had been used on the rear compression side of the weldment to measure the level of the strain during the tests [13]. The specimen was tested in deoxygenated brine for Stress Corrosion Cracking (SCC) in sweet environment (containing 10 bar CO_2, 25% NaCl, pH of 3.3 and Temperature of 110^{o}C). The test condition also featured sodium hydrogen trioxocarbonate, ($NaHCO_3$) which was used as a buffer to adjust the pH level. The welding processes, the 4PBT and the corrosion tests were all carried out at TWI, Cambridge.

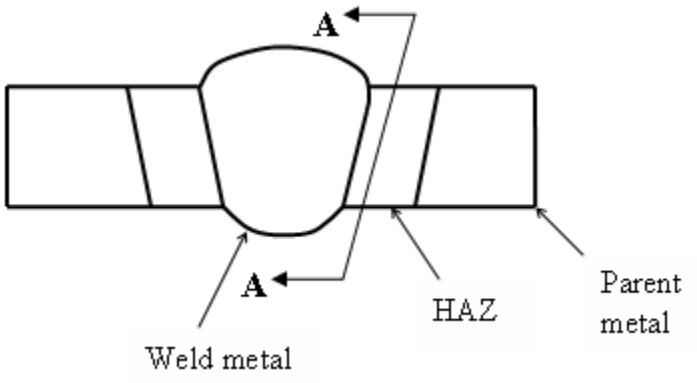

Fig. 1. Weldment showing section A-A parallel to the weld metal in HAZ.

2.4. Optical metallography

The failed sample of the four point bent test was prepared for metallography. Transverse section of dimensions 17×15×3 mm^3 was sectioned from failed 4PT weldment. The specimen was mounted in Bakelite powder on a METASERV automatic mounting press for easy handling. The sample was subsequently grinded with abrasive paper in order of P: 400, 600, 800, 1200 and 4000 grit. The sample was held on abrasive wheel and periodically rotated by 90^{o} to ensure sufficient grinding. Grinding operations were followed by mechanical polishing. The order of diamond grits used for polishing was 1 μm followed by 1/4 μm. Each successive stage of grinding and polishing was followed by washing and drying to avoid contamination.

The specimen was etched by immersion in picral for 3minutes to reveal microstructures in the specimen. The concentration of picral used contained 5g of picric acid and 2.5ml HCl in 100ml ethanol. The etched specimen was rinsed in water and later in ethanol before it was dried with warm air. The specimen was viewed under optical microscope at low magnifications. The different phases in the parent metal, the HAZ and weld metal were examined.

2.5. Transmission electron microscopy of the HAZ

2.5.1. Sample preparation by extraction replica technique

Previous work has shown that the addition of Ti in excess of four times the content of C (see Table 1) will prevent precipitation of carbides at low temperature HAZ but will allow the precipitation to occur in the high temperature

HAZ region close to the fusion boundaries [14]. In recognition of this fact, and to gain access to this region, HAZ of the as-welded specimen was sectioned parallel to the weld metal along section A-A at a distance of approximately 1mm to the weld metal (1). The sectioned area was grinded and polished following the methods described in section 2.3 above. The polished specimen was lightly etched by immersion in picral.

Extraction replica technique was used to prepare direct carbon film specimen of about 20 nm thickness for Transmission Electron Microscopy (TEM). The aim of this technique was to prepare electron transparent specimen impregnated with precipitates of the second phase. The technique was explored to reveal the distribution of carbides on prior austenite grain boundaries in the HAZ.

A single stage direct carbon coating on the etched specimen was carried out using an Edward I (E306) vacuum coating unit, and following the approach developed by [15]. Figure 2 shows schematic illustration of the extraction replica technique used. About 20-30 nm thickness of carbon coating was obtained after 2 minutes at about 10^{-5} torr. The voltage and current of 30 V and 30 A respectively were used during the carbon coating exercise. The coating on the specimen was scored into approximately 2×2 mm^2 to ensure easy stripping of the carbon film during the subsequent electrolytic etching for lift off.

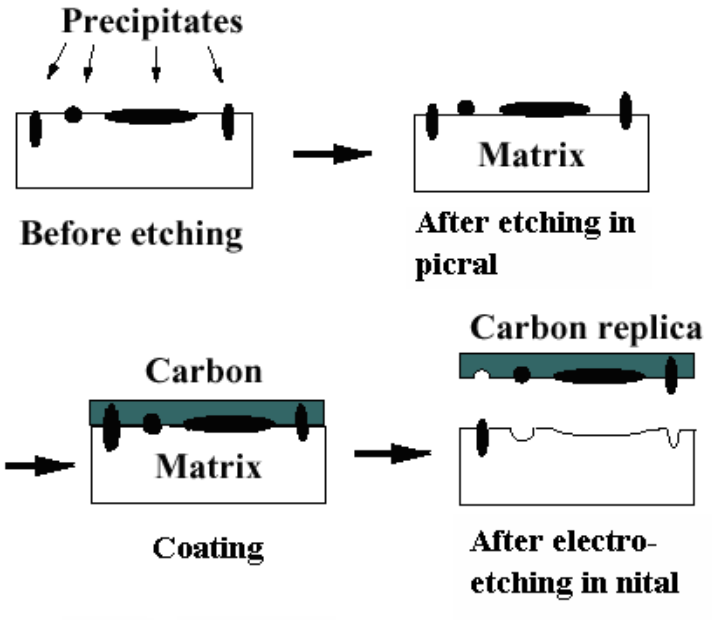

Fig. 2. Schematic demonstrations of extraction replica technique.

The specimen was etched electrolytically in nital, containing 10% nitric acid in 100 ml ethanol, to lift off carbon replica from the surface of the specimen. The replica film floated on the electrolyte and it was carefully collected with spatula and washed in ethanol and then in de-ionised water. The film was collected on 400 mesh 3.05 mm copper grids held with tweezers and ready for Transmission Electron Microscopy.

2.5.2. Energy dispersive x-ray

The specimen was examined in imaging mode of Transmission Electron Microscope (TEM). The model of TEM used was Philips CM 200 electron microscope and was operated at 200 kV. The copper grid containing the specimen was mounted on the single tilt specimen holder of the TEM. Image mode at higher magnification was used to investigate the presence of carbide precipitates on the prior austenite grain boundaries. The chemical composition of the precipitates observed in imaging mode was analysed with Energy Dispersive X-Ray (EDX). The area of high particle density on the grain boundaries was chosen for analysis to achieve a high level of accuracy.

3. Results and Discussion

3.1. Metallographic examination of 4PBT specimen tested in sweet environment

The results of metallographic examination of specimen W2AVII is shown in Figs. 3. Figure 3(a) shows the crack which occurred on the LHS of the weld. The crack propagated close to the fusion boundary in the HAZ and was approximately 1.5mm long. The crack tip later deflected across the HAZ and propagated towards the parent material. There were branches at close range along the main crack path. Cracks occurred on both sides of the weldment.

Figure 3(b) micrograph shows the cracks on the RHS of the weld. The cracks were relatively thin and short compared with the LHS crack. The cracks occurred in the HAZ. They followed zigzag path and also have many branches.

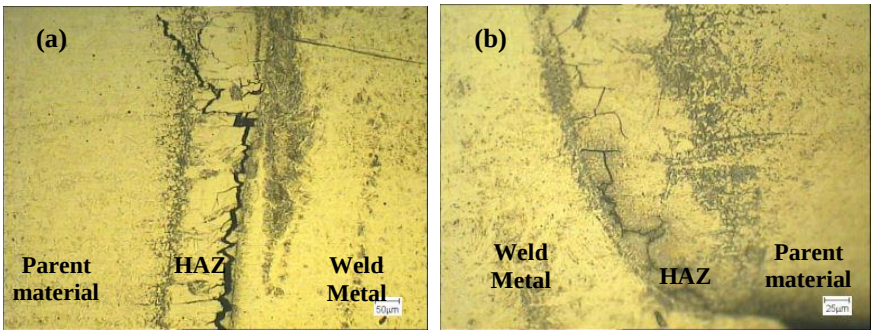

Fig. 3. Optical micrographs of specimen W2AVII tested in sweet environment (etched with picral and aqueous solution of H_2SO_4 and NH_4CNS).

Specimen W2AVII as-received showed cracking on both sides of the weld but evidence of pitting corrosion was not seen with optical microscope. However, the cracks initiated at the weld root and propagated in the HAZ within the neighbourhood of the fusion boundary with characteristic features of intergranular cracking (Fig. 3). The branches along the crack path and the crack tips, Fig. 3(a), are overwhelming evidences of intergranular cracking.

The probable reasons for the severity of the crack in the W2AVII are the higher temperature and acidity of the testing environment. High temperature increases the rate of formation of carbonic acid, Eq. (1), therefore increasing the acidity of the local environment.

$$CO_2 + H_2O \Leftrightarrow H_2CO_3 \quad (1)$$

The presence of carbonic acid lowers the pH of the water in the system and it provides hydrogen ion as electron acceptors. The reduction in pH or the amount of carbonic acid is depended primarily upon the pressure at which the system is been operated. The rate of corrosion increases with increase in partial pressure of CO_2. But, the presence of some dissolved minerals in the environment may act as buffering agent to subjugate the reduction of pH level in the system. The formation of carbonic acid is a very slow process and the corrosion rate is expected to be slow at room temperature. But at elevated temperature, the severity of corrosion in CO_2 environment increases with rise in temperature.

The occurrence of intergranular cracks in specimen W2AVII is consistent with the mechanism of sensitization. Sensitization occurred as a result of precipitation Cr carbides preferentially along the prior austenite grain boundaries and in effect, leading to depletion of Cr content to the level below the requirement for corrosion resistance of the steel [2, 12, 16]. The presence of carbides on the grain boundaries with a resultant low level of Cr within the immediate vicinity of the precipitates may make the grain boundaries to be anodic to its surrounding. Eventually, micro-galvanic corrosion may occur as a result of this process and the material becomes more susceptible to Intergranular Stress Corrosion (IGSCC).

On the other hand, the high density of C and N in the weld metal as a result of super duplex stainless steel filler may allow diffusion of these elements across the fusion boundaries into the high temperature HAZ. The C and N enrichment may be another justification for sensitization in the neighbourhood of fusion boundary region where the crack propagation was more dominant. The reason for the crack deflection towards the parent metal, as shown in Fig. 3(a), was not entirely clear, however, this could be attributed to the grain orientation and possibility the deflection of the intergranular crack may have occurred at grain boundaries triple joints. Again, the deflection of crack paths could be assisted by high hardness of the HAZ [17] since the crack was later arrested by relatively ductile parent metal. This explains the reason for the occurrence of intergranular cracking in specimen W2AVII. The observation of crack in the HAZ and the proposition of the sensitisation mechanism as the justification for the crack, necessitate the use of TEM for probing the prior austenite grain boundaries for precipitate and its chemical analysis.

3.2. Transmission electron microscopy

The transmission electron micrographs of extraction replica are shown in Figs. 4(a) and (b). The results confirmed the presence of precipitates clusters aligned on the prior austenite grain boundaries. There were scanty particles within the grain matrix, some of which were relatively smaller in size. The average size of the

precipitates was about 20 nm diameter. The result of compositional analysis of the precipitates with Energy Dispersive X-ray during TEM imaging is shown in Fig. 5. The EDX result showed the presence of Chromium, Iron, Copper and Molybdenum (though very small but it presence in the background was registered). The large amount of Cu in the spectrum was because of fine 400 mesh copper grid used to collect the carbon film. From the results of the EDX, it was therefore suggested that the precipitates were probably chromium-iron carbides of the form $M_{23}C_6$. These results are consistent with similar works of Hara and Asahi [18] and Rogne et al. [19].

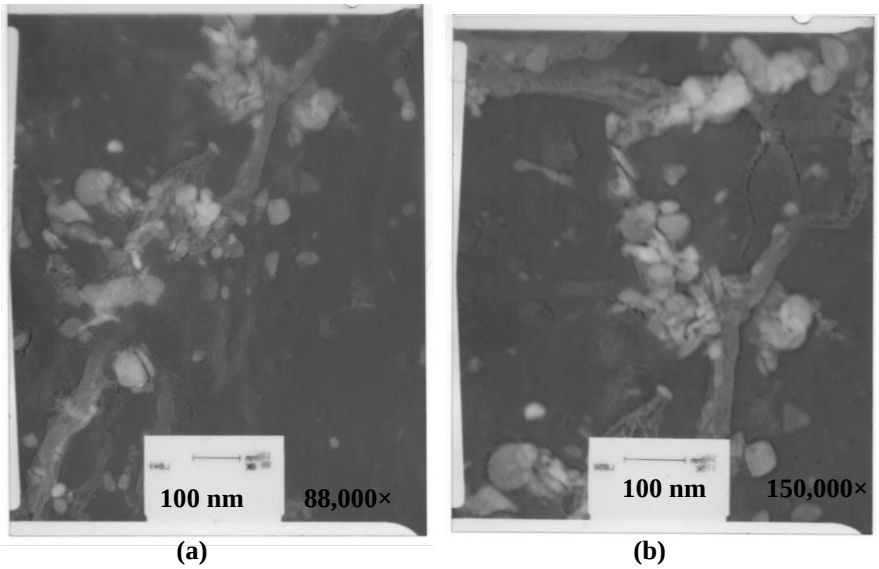

Fig. 4. Transmission electron micrographs of extraction replica.

Figures 4(a) and 4(b) show bright field image of extraction replicas of the as-welded specimen taken at magnification of 88,000× and 150,000× respectively. The micrographs were taken at locations in the HAZ of the as-welded specimen close to the weld root.

The precipitation of Cr-Fe carbides of the form $M_{23}C_6$ preferentially along the prior austenite grain boundary is strongly supported by this study and may be responsible for the observed intergranular corrosion in Fig. 3. Sensitization occurs as a result of depletion of Cr within the neighbourhood of carbides to a level below the requirement for corrosion protection. This may set up micro-galvanic corrosion along the grain boundary and eventually allowing greater susceptibility to intergranular failure. The probable remedial measure in addition to careful postweld heat treatment [20] to minimise sensitisation is to increase the amount of titanium in the alloy composition of the MSS. Titanium helps to stabilise the much needed chromium for corrosion protection on account of higher affinity of carbon for titanium than chromium [21]

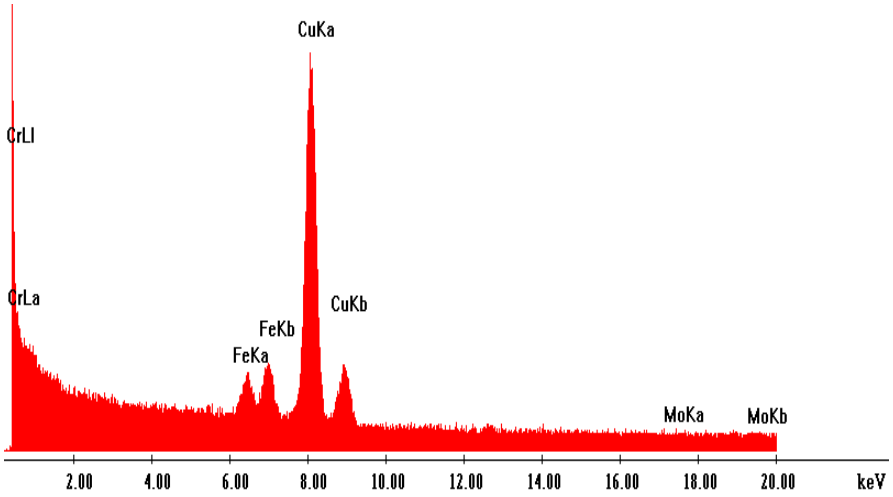

Fig. 5. EDX analysis of particles on prior austenite grain boundaries.

4. Conclusions

The following conclusions are made at the end of the study on the analysis of intergranular carbide precipitate in HAZ of martensitic stainless steel with transmission electron microscopy.

- It was discovered that super duplex weld metal contained high amount of carbon and nitrogen which diffuse across the narrow fusion boundary into the neighbouring heat affected zone (with an initial relatively low concentration). The resulting carbon and nitrogen enrichment of the heat affected zone material.
- Carbon enrichment of the heat affected zone close to the weld metal may increase the propensity for chromium carbide precipitation at grain boundaries and hence the degree of sensitization and susceptibility to intergranular stress corrosion cracking.
- The specimen tested in a sweet environment showed cracks which are dominated by intergranular features. The explanation for intergranular stress corrosion cracking is most likely to relate to the observation of grain boundary carbides in the Heat Affected Zone, leading to chromium depletion in this region, i.e., local grain boundary sensitization.
- Transmission Electron Microscopy showed evidence of carbide precipitate on the grain boundaries and this corroborates the mechanism of intragranular cracking propagation by sensitisation.
- The Energy Dispersive X-ray analysis of precipitates observed on the grain boundaries showed the presence of chromium and molybdenum thereby suggesting the carbide was of the form $M_{23}C_6$.

Acknowledgements

The authors wish to thank Dr Alan Harvey of Manchester Materials Science Centre for the technical support on the use of TEM. The supply of samples by

TWI, Cambridge and the technical supports received in areas of fabrication and experimental tests were duly acknowledged. The logistic support of Miss Sophia O. Necib is duly acknowledged.

References

1. Griffiths, A.; Nimmo, W.; Roebuck, B.; Hinds, G.; and Turnbull, A. (2004). A novel approach to characterising the mechanical properties of supermartensitic 13 Cr stainless steel welds. *Materials Science and Engineering, A*, 384(1-2), 83-91.
2. Turnbull, A.; and Griffiths, A. (2003). Review: Corrosion and cracking of weldable 13 wt-% Cr martensitic stainless steels for application in the oil and gas industry. *Corrosion Engineering, Science and Technology*, 38(1), 21-50.
3. Enerhaug, J.; and Steinsmo, U. (2001). Factors affecting initiation of pitting corrosion in super martensitic stainless steel weldments. *Science and Technology of Welding & Joining*, 6(5), 330-338.
4. Liu, Z.Y.; Wang, X.Z.; Liu, R.K.; Du, C.W.; and Li, X.G. (2014). Electrochemical and sulfide stress corrosion cracking behaviors of tubing steels in a h2s/co2 annular environment. *Journal of Materials Engineering and Performance*, 23(4), 1279-1287.
5. Bai, B.; Zhang, C.; Wang, J.; Tong, Z.; Lv, Q.; and Yang, W. (2016). Thermal aging effect of 17-4ph martensitic stainless steel valves for nuclear power plant. in *Materials Science Forum*.
6. Ahmed, I.I.; Grant, B.; Sherry, A.H.; and Quinta da Fonseca, J. (2014). Deformation path effects on the internal stress development in cold worked austenitic steel deformed in tension. *Materials Science and Engineering: A*, 614(0), 326-337.
7. Messler, R.W. (2008). *Principles of welding: Processes, physics, chemistry, and metallurgy*. John Wiley & Sons.
8. Aquino, J.M.; Della Rovere, C.A.; and Kuri, S.E. (2009). Intergranular corrosion susceptibility in supermartensitic stainless steel weldments. *Corrosion Science*, 51(10), 2316-2323.
9. Dahmen, M.; Rajendran, K.D.; and Lindner, S. (2015). Sensitization of laser-beam welded martensitic stainless steels. *Physics Procedia*, 78, 240-246.
10. Kvaale, P.E.; and Olsen, S. (1999). Experience with supermartensitic stainless steels in flowline applications. In *Stainless Steel World 99 KCL Publishing BV*.
11. Woollin, P. (2007). Welding supermartensitic stainless steels for corrosive service. in *Stainless Steel World Conference, Maastricht, Holanda*.
12. Woollin, P. (2007). Postweld heat treatment to avoid intergranular stress corrosion cracking of supermartensitic stainless steels. *Welding in the World*, 51(9-10), 31-40.
13. Woollin, P.; Noble, D.N.; and Lian, B. (1999). Weldable 13%Cr martensitic steels for pipeline applications: Preliminary studies. In *EPRG/PRCI 12th Biennial Joint Technical Meeting on Pipeline Research*.
14. Lancaster, J.F. (1999). *Metallurgy of welding*. Elsevier.

15. Bradley, D. (1954). Evaporated carbon films for use in electron microscopy. *British Journal of Applied Physics*, 5(2), 65.
16. Woollin, P.; and Carrouge, D. (2002). Heat affected zone microstructures in supermartensitic stainless steels. in *Conference on Super martensitic Stainless Steels, Bruxelas, Bélgica*.
17. Ahmed, I.; Adebisi, J.; Yahaya, T.; Abdulkareem, S.; and Sherry, A. (2016). Microstructural correlation of hardness profile in martensitic stainless steel weldment. *Metallography, Microstructure, and Analysis*, 5(1), 43-49.
18. Hara, T.; and Asahi, H. (2000). Effect of d d-ferrite on sulfide stress cracking in a low carbon 13 mass% chromium steel. *ISIJ international*, 40(11), 1134-1141.
19. Rogne, T.; Lange, H.I.; Svenning, M.; Aldstedt, S.; Ladanova, E.; Solberg, J.K.; Olsen, S.; Howard, R.; and Leturno, R.E. (2002). Intergranular corrosion/cracking of weldable 13% Cr steel at elevated temperature. In *Corrosion*. Houston, Texas: *NACE International*.
20. Mirakhorli, F.; Cao, X.; Pham, X.-T.; Wanjara, P.; and Fihey, J.-L. (2016). Post-weld tempered microstructure and mechanical properties of hybrid laser-arc welded cast martensitic stainless steel CA6NM. *Metallurgical and Materials Transactions B*, 47(6), 3245-3256.
21. Alvarez, C.; Almanza, E.; and Murr, L. (2005). Evaluation of the sensitization process in 304 stainless steel strained 50% by cold-rolling. *Journal of Materials Science*, 40 (11), 2965-2969.